NANO LETTERS
Cite This: Nano Lett. 2018, 18, 853−858
Letter
pubs.acs.org/NanoLett

Surpassing Single Line Width Active Tuning with Photochromic Molecules Coupled to Plasmonic Nanoantennas

Wade M. Wilson,[†,‡] Jon W. Stewart,[†,‡] and Maiken H. Mikkelsen*[,†,‡,§]

[†]Center for Metamaterials and Integrated Plasmonics, [‡]Department of Electrical and Computer Engineering, and [§]Department of Physics, Duke University, Durham, North Carolina 27708, United States

Supporting Information

ABSTRACT: Active plasmonic nanostructures with tunable resonances promise to enable smart materials with multiple functionalities, on-chip spectral-based imaging and low-power optoelectronic devices. A variety of tunable materials have been integrated with plasmonic structures, however, the tuning range in the visible regime has been limited to less than the line width of the resonance resulting in small on/off ratios. Here we demonstrate dynamic tuning of plasmon resonances up to 71 nm through multiple cycles by incorporating photochromic molecules into plasmonic nanopatch antennas. Exposure to ultraviolet (UV) light switches the molecules into a photoactive state enabling dynamic control with on/off ratios up to 9.2 dB and a tuning figure of merit up to 1.43, defined as the ratio between the spectral shift and the initial line width of the plasmonic resonance. Moreover, the physical mechanisms underlying the large spectral shifts are elucidated by studying over 40 individual nanoantennas with fundamental resonances from 550 to 720 nm revealing good agreement with finite-element simulations.

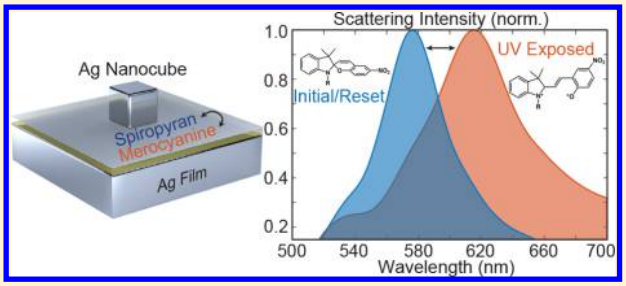

KEYWORDS: *Dynamic tuning, nanocube, photoswitching, plasmonics, photochromic, single particle spectroscopy*

Metallic nanostructures with subwavelength features enable unprecedented control of interactions between optical waves and nanoscale materials through the exploitation of localized surface plasmon resonances. Localized surface plasmons confine the incident optical energy into deeply subwavelength volumes producing large electric and magnetic field enhancements causing the plasmons to be particularly sensitive to the local environment and geometry. Customarily, plasmonic nanostructures are embedded in a static environment effectively fixing the plasmon resonance which can only be changed by refabricating the device or inducing permanent morphological changes.[1,2] Incorporating active materials with plasmonic nanostructures promises to provide novel dynamic optical materials with full reversibility, repeatability, and ultrafast response times. Previous demonstrations of active tuning have leveraged changes in the local dielectric environment surrounding the nanostructure or a change in the geometry. Modification of the dielectric environment around plasmonic nanostructures alters the dispersion at the metal−dielectric interface thus altering the plasmon resonance wavelength. Similarly, localized surface plasmon resonances depend upon the geometry of the metallic surface and thus small modifications in the geometry can lead to large resonance shifts. Active tuning has been achieved using various techniques including (i) phase change materials,[3−8] (ii) direct electrical and optical variation of the dielectric constants in the material surrounding the nanostructure,[9−17] and (iii) mechanical, chemical, or thermal deformation of the physical structure of the device.[18−26] These techniques show significant promise, however, they have been either restricted to the infrared regime[3−12] or suffer from limitations in regards to reversibility[18−25] and tuning range.[17,20,21,23] Additionally for applications in on-chip light sources, optical switching, and optical computing, an all-optical tuning scheme is highly desirable. Recent demonstrations of all-optical tuning of plasmonic nanostructures with weak incident fields have achieved shifts up to 32 nm[27−30] but depend upon large, spatially extended lattice and surface plasmon modes not ideal for compact, on-chip devices.

Here we demonstrate reversible photoisomerization of photochromic molecules integrated into plasmonic nanopatch antennas consisting of film-coupled silver nanocubes. The plasmonic resonance of individual nanoantennas was reversibly tuned up to 71 nm in the visible regime by exposing the photochromic molecules in the nanocavity with UV light to induce a photoisomerization reaction. Resetting the isomerization process was realized with white light exposure. Single particle spectroscopy measurements verified the tuning of individual nanopatch antennas before and after the photoisomerization process. The large experimental tuning as confirmed through finite-element simulations results from

Received: September 23, 2017
Revised: December 15, 2017
Published: December 28, 2017

DOI: 10.1021/acs.nanolett.7b04109
Nano Lett. 2018, 18, 853−858

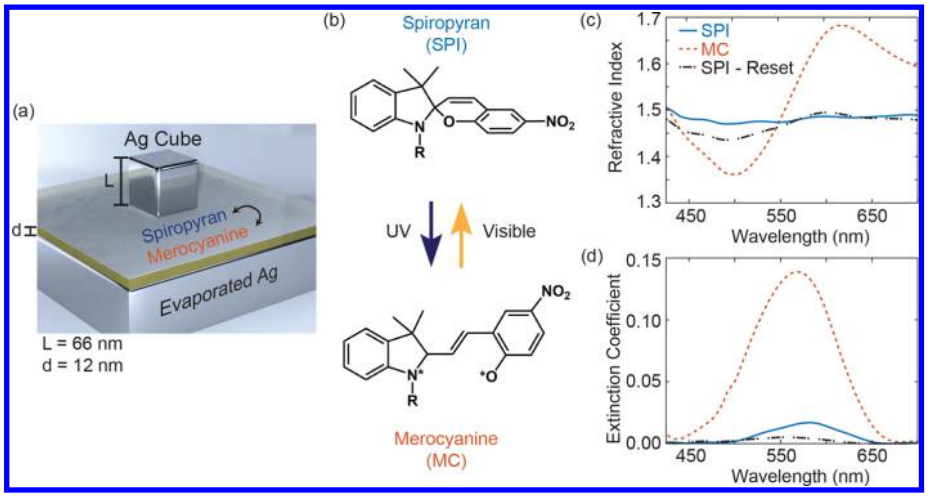

Figure 1. (a) Schematic of film coupled nanopatch antenna with 66 nm nanocube and 12 nm photochromic spacer layer over a 75 nm silver film. (b) Chemical structure diagram showing two isomers of SPI that can be alternated through either UV or visible light exposure. (c,d) Refractive index and extinction coefficient of a 12 nm layer of SPI/PMMA before (blue "SPI") and after UV exposure (red "MC") and after being thermally reset (yellow "SPI-Reset").

resonant coupling of the plasmonic resonance with the photochromic molecules after photoisomerization.

The plasmonic nanoantennas are comprised of silver nanocubes separated from a silver film by a composite spiropyran (SPI) and poly(methyl methacrylate) (PMMA) spacer layer as shown in Figure 1a. They act as both a small mode volume nanocavity for extreme field confinement and a nanopatch optical antenna for efficient coupling of light to localized plasmons. The fundamental resonance of this structure shown in the electric field profile of Figure 2a depends strongly on the nanocube size, gap layer thickness, and the dielectric properties of the material in the gap.[31−33] The controllable optical properties of the SPI thin films make them ideal candidates for altering the resonance of these nanostructures. The thin films were prepared by spin coating 3:2 weight ratio solutions of SPI and PMMA in anisole onto a 75 nm template-stripped silver film. A subnanometer layer of cationic poly(allylamine hydrochloride) (PAH) was self-assembled onto the SPI-PMMA thin film to facilitate better adhesion of the anionic poly(vinylpyrrolidone) (PVP) coated silver nanocubes. The colloidal silver nanocubes were then drop-casted and electrostatically adhered to the PAH polymer layer using a dilute solution of nanocubes to ensure that only a single nanoantenna is contained within a diffraction limited spot. A more detailed fabrication procedure is described in the Sample Fabrication Section of the Supporting Information. Figure 1b shows the chemical structure of the photochromic isomers before and after UV exposure and depicts the C—O ring opening reaction that induces the change in optical properties. The photoisomerization to merocyanine (MC) can be reversed through visible light or thermal exposure and the switching process can be repeated.[35] The optical characteristics of 12 nm thick SPI-PMMA films were probed using variable angle spectroscopic ellipsometry. The optical parameters were extracted from fitting the ellipsometry data to a Lorentzian oscillator model and the results are consistent with previously reported data.[27−29,34−37] Figure 1c,d shows the refractive index and extinction coefficient before and after the photoisomerization reactions. The data clearly shows a significant change in the refractive index centered around 550 nm coinciding with a large increase in the extinction coefficient with a peak at 560 nm. Ellipsometry measurements allowed for the characterization of damage and switching thresholds prior to integration with the plasmonic structure. The switching threshold for the 3:2 SPI-PMMA thin films was found to be a 4 min exposure using a 340 nm light-emitting diode (LED) at an ~1 mW/cm^2

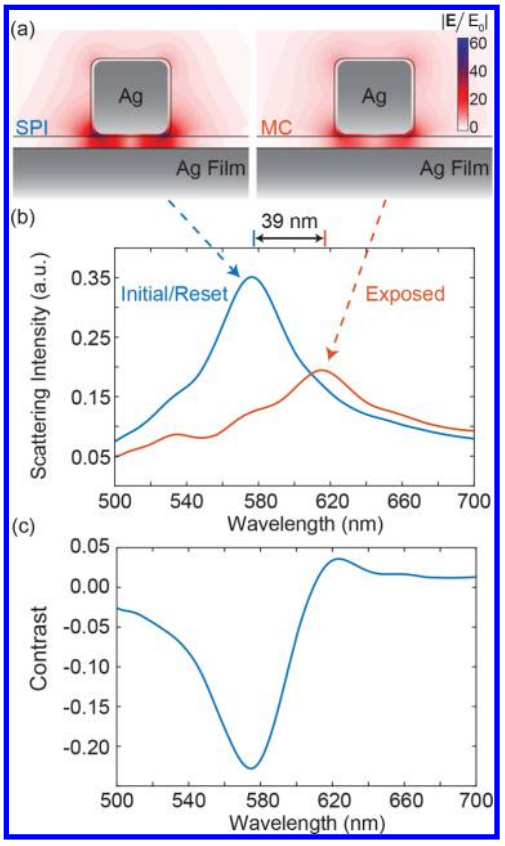

Figure 2. (a) Simulated electric field enhancement for nanoantennas with SPI and MC in the gap region shown at the fundamental resonance (565 and 610 nm, respectively). (b) Representative nanoantenna dark-field scattering spectra taken before and after UV exposure. (c) Contrast between scattering spectra taken before and after UV exposure.

DOI: 10.1021/acs.nanolett.7b04109
Nano Lett. 2018, 18, 853−858

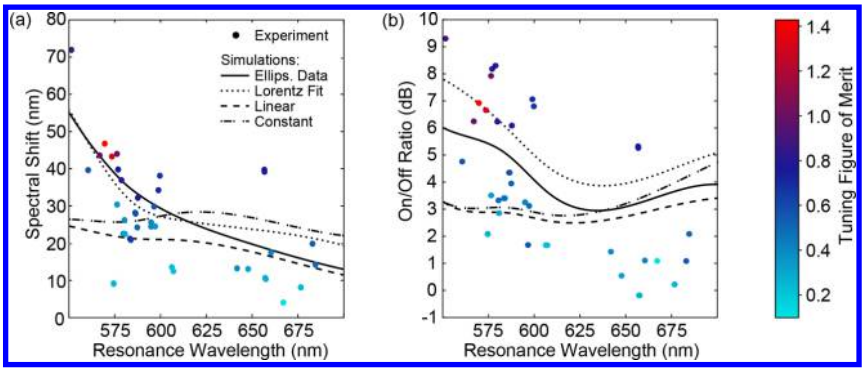

Figure 3. (a) Experimental and simulated change in the peak scattering wavelength for nanoantennas with different resonance wavelengths. (b) Experimental and simulated on/off ratio for nanoantennas with different resonance wavelengths. The colors of the data points indicate the tuning figure of merit (spectral shift divided by the fwhm of the initial resonance). The simulation labels denote different dispersion models for the refractive index of MC. The dispersion in refractive index and extinction coefficient used for the "Ellips. Data" simulation was taken from ellipsometry measurements on a thin SPI(MC)-PMMA film. The "Lorentz Fit" simulation used an ideal Lorentzian oscillator fit of the ellipsometry data. The "Linear" and "Constant" simulations used linear dispersion and a dc shift in the refractive index respectively, with no extinction.

power density as described in Figure S2 of the Supporting Information.

As depicted in Figure 2, the fundamental resonance of the plasmonic nanoantenna can be tuned by incorporating the photochromic thin film into the gap region and exposure to UV light to induce the photoisomerization process. Figure 2a shows the simulated electric field enhancement of the fundamental plasmonic mode before and after photoisomerization for a nanoantenna composed of a 75 nm silver film, a 10 nm SPI-PMMA film and a 66 nm cube with a 3 nm PVP coating. The field enhancements are calculated by dividing the magnitude of the electric field vector, denoted as **E**, by the incident field magnitude, E_0, used to excite the resonance. The simulations demonstrate the effect of the SPI and MC isomers on the fundamental plasmonic mode, where the maximum field enhancement reached 60 times for the SPI case and 38 times for the MC case. The smaller simulated field enhancements for the MC simulations arise from the increased extinction coefficient of MC evident in Figure 1d, which introduces higher losses into the system resulting in a weaker plasmonic resonance. Experimentally, single particle spectroscopy measurements were taken of the plasmonic nanoantennas before and after UV exposure using a custom-built microscope depicted in Figure S1 of the Supporting Information. The UV LED was integrated into the microscope with a power density between 0.99 and 1.07 mW/cm^2 and a 10.6 μm diameter excitation spot size. Each nanoantenna was identified using an EM-CCD camera with bandpass filters around the resonance of the nanostructures. Once identified, a white light scattering spectrum was taken by integrating over an area with a 3 μm diameter on the sample. Next, the nanoantennas were irradiated with UV light for 10 min to ensure full conversion of the SPI molecules to MC, and another white light scattering spectrum was taken to compare to the initial scattering resonance. After blocking the UV light, another spectrum was taken after 10 min of exposure to white light to verify the reversibility of the switching process. Figure 2b shows the experimental data from exposing a representative single nanoantenna with a resonance initially centered at 577 nm. The nanoantenna was composed of a 75 nm silver film, a 12 nm PMMA/SPI spacer, a subnanometer polymer adhesion layer, and a silver nanocube with a 66 nm nominal side length. After UV exposure, the resonance of the nanoantenna was spectrally shifted by 39 nm which corresponds to 0.75 times the full width at half-maximum (fwhm) of the initial resonance often denoted as the tuning figure of merit (FOM, spectral shift divided by the fwhm of the initial spectrum). The decreased scattering intensity between the initial resonance and switched resonance is due to resonant coupling of the plasmonic resonator to the MC isomer which introduces losses to the system. Figure 2c shows the contrast between the initial and switched nanoantenna states defined as the difference between their scattering intensities. At the initial resonance wavelength, the contrast is 65%, while at the switched resonance the contrast is 13%. The simulations and experimental data in Figure 2b,c both depict that the photoisomerization reaction shifts and damps the fundamental mode of the plasmonic nanoantennas.

To elucidate the mechanisms underlying the large peak wavelength shifts and investigate the effect of resonant coupling between the nanoantennas and MC, the resonance wavelength of the nanoantennas was varied. For this investigation, nanoantennas with a fundamental resonance between 550 and 720 nm were fabricated by altering the thickness of the SPI-PMMA film from 2 to 25 nm and through the inherent size distribution of the 66 $\pm$ 5 nm silver nanocubes. Through this, the dependence between the tuning range and the gap thickness of the nanoantenna is investigated while keeping the nanocube size fixed within 7.5%. Switching data was taken for 41 individual nanoantennas across the visible spectrum. Figure 3a depicts the analyzed experimental data where each point corresponds to a single plasmonic nanoantenna plotted according to its resonance wavelength and amount of spectral shift. The color of each data point indicates the FOM for the nanoantenna calculated from the line width of the initial resonance. The FOM was selected as a representation of the quality of tuning due to its isolation of the spectral switching properties from the absolute scattering intensity. Figure 3a shows that as the resonance wavelength is blue-shifted toward 550 nm the spectral shift increases. Furthermore, the FOM is the highest for nanoantennas with a 12 nm film thickness and resonance wavelengths near 570 nm. Thicknesses beyond 25 nm result in nanoantennas that are poorly coupled to the metallic substrate and cannot blue shift the resonance beyond 550 nm. Figure 3b shows the scattering on/off ratio at the initial resonance for the same nanoantennas shown in Figure 3a and similarly depicts the FOM with their respective color. Similar to the spectral shift, the on/off ratio exhibits increased performance for blue-shifted resonances. It is important to note

DOI: 10.1021/acs.nanolett.7b04109
Nano Lett. 2018, 18, 853−858

that if the scattering intensity and fwhm do not change upon switching, the on/off ratio will be directly related to the FOM. However, because the scattering fwhm and the intensity do change upon photoisomerization as shown in Figure 2b and Figure S4, the nanoantennas with the highest FOM do not necessarily have the highest on/off ratios. The largest spectral shift and on/off ratio occurs for the nanoantenna with its initial resonance centered at 550 nm, which exhibits 71 nm of spectral shift and 9.2 dB of selectivity. On average, the highest on/off ratios, FOMs, and spectral shifts arise from nanoantennas with initial resonances centered between 550 and 580 nm coinciding with the molecular transition of the MC isomer. To the first order when the index of refraction in a plasmonic gap changes, there is a corresponding change in the plasmon resonance. From this, it would be expected that the largest spectral shifts and on/off ratios would be observed when the nanoantenna resonance overlaps with the largest refractive index change between the SPI and MC isomers at 615 nm. However, the largest spectral shifts and on/off ratios observed experimentally occur around the minimal change in the index of refraction near 550 nm, suggesting that a more complex phenomenon is responsible for the large spectral shifts.

For further insight into the mechanisms underlying the large experimental tuning, finite-difference frequency domain (FDFD) finite-element scattering simulations were conducted utilizing varying dispersion models for the refractive index of MC. The simulation results are overlaid with the experimental data in Figure 3a,b where the solid and dashed black lines correspond to the scattering simulations for 66 nm nanocubes with 2−12 nm spacer thicknesses and are labeled according to the dispersion profile used for the MC-PMMA refractive indices. The different dispersion profiles are plotted in Figure S1 of the Supporting Information along with the simulation results. The constant dispersion profile uses the largest index change at 615 nm in the ellipsometry data and models the photoisomerization reaction as a constant index change from 1.49 to 1.68 over the entire wavelength range. The linear dispersion profile is similar but accounts for the negative dispersion of the MC not included in the constant dispersion case. Simulations utilizing the ellipsometry data from Figure 1c,d for the refractive index of the spacer layer agrees well with the observed experimental spectral shifts and on/off ratios. Fitting the ellipsometry data with a Lorentzian oscillator dispersion model similarly results in good agreement with the experimental data. The Lorentzian dispersion model was chosen to enable investigation of the macroscopic effects of dipolar coupling of the MC molecules to the plasmonic mode. The Lorentzian dispersion model is a homogenized material response derived from assuming the material is comprised of many dipoles within a subwavelength volume, which as seen in Figure 3a,b is a good approximation for the dense MC-PMMA photochromic films used in this work. Comparing the simulation results using these four dispersion profiles it is further evident that the nanoantenna tuning does not directly result from a change in refractive index in the gap region.

As shown in Figure 3a, the linear and constant dispersion models consistently underestimate the amount of spectral shift at wavelengths near the transition of MC. The overlay of the simulations with experimental results in Figure 3a,b shows that the large spectral shifts observed in this work are described better by the refractive index profiles modeled with a resonant dipolar response centered at 550 nm. Figure S3 in the Supporting Information further reveals that the fwhm and intensity change is greatest between the initial and switched resonances for nanoantennas that are better coupled to the lossy MC isomer. The good agreement between experiment and simulations that used a Lorentzian oscillator to model a resonant dipole with respect to the spectral shift, on/off ratio, intensity change, and line width broadening of the plasmonic resonances leads to the conclusion that the mechanism responsible for the large tuning demonstrated here is weak-coupling between the MC isomer and the fundamental plasmonic resonance. As the plasmonic resonance and the resonance of the MC isomers are overlapped, the coupling strength increases and larger spectral shifts are observed despite minimal change in the index. Because no characteristic evidence of strong coupling is observed, such as peak splitting and anticrossings as shown in other recent demonstrations,[27,28] the MC isomers are most likely weakly coupled to the plasmonic resonator. However, the switchable resonant coupling shown here results in larger spectral shifts and on/off ratios as compared to nonresonant changes in refractive index at the expense of increased losses.

Beyond the tuning mechanisms, another important aspect to characterize with dynamic devices is the reversibility beyond a single switching cycle. In this work, ellipsometry was used to evaluate the performance of the SPI/MC isomerization for several switching-reset cycles. Using the same switching parameters as described earlier, Figure 4a demonstrates the extinction coefficient alteration of the MC/PMMA composite through four consecutive switching cycles, labeled respectively

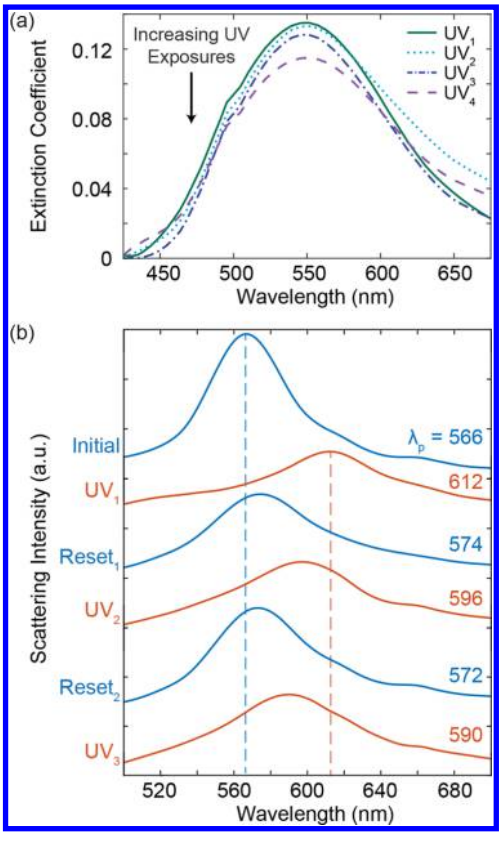

Figure 4. (a) Extinction coefficient extracted from ellipsometry measurements after multiple UV exposure- reset cycles. (b) Scattering spectra from a representative nanoantenna after multiple UV exposure-white light reset cycles, where λ_p denotes the wavelength where peak scattering intensity occurs.

DOI: 10.1021/acs.nanolett.7b04109
Nano Lett. 2018, 18, 853−858

as UV_{1-4}. It is seen that after these four cycles the extinction coefficient decreases by 14% relative to the initial switch, indicating fatigue of the SPI molecules. The fatigue of SPI from UV exposure is a result of side reactions leading to modified molecular structures with a lack of photoresponsive properties.[35] It is important to note, the fatigue of SPI is minimized when embedded in PMMA as compared to other polymer host matrices.[34] The fatigue evident in the ellipsometry data is similarly seen in reduced spectral shifts of the nanoantenna after multiple cycles as shown in Figure 4b. The scattering resonance of a single nanoantenna is shown through three cycles with a 62% reduction in the spectral shift after the third cycle. The increased fatigue in the nanoantenna is most likely a result of the extreme environment in the nanometer-scale plasmonic cavity and due to accumulation of semistable but optically inert isomers of SPI. When reset thermally these states can be eliminated but using visible light to revert the MC back to SPI does not fully recover all the molecules in the time scale of 10 min. Other photoswitchable molecules have greater fatigue resistance but exhibit smaller changes in the optical constants upon photoisomerization.[38]

In conclusion, we have demonstrated reversible tuning of the plasmon resonance of over 40 distinct nanoantennas in the visible regime through the photoisomerization of SPI integrated between silver nanocubes and a silver film. The plasmon resonance was actively tuned over multiple cycles by up to 71 nm corresponding to a FOM of 1.43 which to the best of our knowledge is the highest reported in the visible spectrum. The scattering spectra of single nanoantennas were actively redshifted by varying amounts depending on their initial resonance wavelength and nanoparticle size, correlating with the coupling strength between the MC isomers and the plasmonic resonance. The experimental results show good agreement with finite-element simulations, demonstrating dynamic control over plasmon resonances with an all optical approach. Furthermore, the inherent switching rate of SPI isomers to MC in solution have been shown to surpass 40 ps[39] promising for applications requiring ultrafast tuning with high on/off ratios.

■ ASSOCIATED CONTENT

Supporting Information

The Supporting Information is available free of charge on the ACS Publications website at DOI: 10.1021/acs.nanolett.7b04109.

Details and methods of finite-element COMSOL simulations; simulations of different dispersion profiles of MC integrated into nanoantennas; detailed sample fabrication procedure; setup and diagram of dark-field scattering microscope; characterization of photochromic switching parameters; changes of scattering intensity and fwhm according to initial plasmonic resonance (PDF)

■ AUTHOR INFORMATION

Corresponding Author

*E-mail: m.mikkelsen@duke.edu. Phone: +1 (919) 660-0185.

ORCID

Maiken H. Mikkelsen: 0000-0002-0487-7585

Author Contributions

W.M.W. and J.W.S. contributed equally to this work. W.M.W. and J.W.S. performed the ellipsometry measurements. W.M.W. performed the scattering measurements. J.W.S. completed the finite-element simulations. W.M.W. and J.W.S. analyzed the data. M.H.M., W.M.W., and J.W.S. wrote the manuscript, M.H.M. designed and supervised the project, All authors discussed the results and commented on the manuscript.

Notes

The authors declare no competing financial interest.

■ ACKNOWLEDGMENTS

Support is acknowledged from the Army Research Office Young Investigator Research Program (ARO, Grant W911NF-16-1-0471) and the Air Force Office of Scientific Research Young Investigator Research Program (AFOSR, Grant FA9550-15-1-0301).

■ REFERENCES

(1) Lumdee, C.; Toroghi, S.; Kik, P. *ACS Nano* **2012**, *6*, 6301−6307.
(2) Zhu, X.; Vannahme, C.; Højlund-Nielsen, E.; Mortensen, A. N.; Kristensen, A. *Nat. Nanotechnol.* **2015**, *11*, 325−329.
(3) Earl, S.; James, T.; Davis, T.; McCallum, J.; Marvel, R.; Haglund, R.; Roberts, A. *Opt. Express* **2013**, *21*, 27503.
(4) Michel, A.-K.; Zalden, P.; Chigrin, D.; Wuttig, M.; Lindenberg, A.; Taubner, T. *ACS Photonics* **2014**, *1*, 833−839.
(5) Kocer, H.; Butun, S.; Banar, B.; Wang, K.; Tongay, S.; Wu, J.; Aydin, K. *Appl. Phys. Lett.* **2015**, *106*, 161104.
(6) Lei, D.; Appavoo, K.; Sonnefraud, Y., Jr; H, R. *Opt. Lett.* **2010**, *35*, 3988.
(7) Abate, Y.; Marvel, R.; Ziegler, J.; Gamage, S.; Javani, M.; Stockman, M.; Haglund, R. *Sci. Rep.* **2015**, *5*, 13997.
(8) Yin, X.; Schäferling, M.; Michel, A.-K.; Tittl, A.; Wuttig, M.; Taubner, T.; Giessen, H. *Nano Lett.* **2015**, *15*, 4255−4260.
(9) Yang, Y.; Kelley, K.; Sachet, E.; Campione, S.; Luk, T.; Maria, J.-P.; Sinclair, M.; Brener, I. *Nat. Photonics* **2017**, *11*, 390−395.
(10) MacDonald, K.; Sámson, Z.; Stockman, M.; Zheludev, N. *Nat. Photonics* **2009**, *3*, 55−58.
(11) Guo, P.; Schaller, R.; Ketterson, J.; Chang, R. *Nat. Photonics* **2016**, *10*, 267−273.
(12) Abb, M.; Albella, P.; Aizpurua, J.; Muskens, O. *Nano Lett.* **2011**, *11*, 2457−2463.
(13) Kim, J.; Son, H.; Cho, D. J.; Geng, B.; Regan, W.; Shi, S.; Kim, K.; Zettl, A.; Shen, Y.-R.; Wang, F. *Nano Lett.* **2012**, *12*, 5598−5602.
(14) Yi, F.; Shim, E.; Zhu, A.; Zhu, H.; Reed, J.; Cubukcu, E. *Appl. Phys. Lett.* **2013**, *102*, 221102.
(15) Vardi, Y.; Cohen-Hoshen, E.; Shalem, G.; Bar-Joseph, I. *Nano Lett.* **2016**, *16*, 748−752.
(16) Müller, J.; Sönnichsen, C.; von Poschinger, H.; von Plessen, G.; Klar, T.; Feldmann, J. *Appl. Phys. Lett.* **2002**, *81*, 171−173.
(17) Chu, K.; Chao, C.; Chen, Y.; Wu, Y.; Chen, C. *Appl. Phys. Lett.* **2006**, *89*, 103107.
(18) Duan, X.; Kamin, S.; Liu, N. *Nat. Commun.* **2017**, *8*, 14606.
(19) Wang, G.; Chen, X.; Liu, S.; Wong, C.-P. P.; Chu, S. *ACS Nano* **2016**, *10*, 1788.
(20) König, T.; Ledin, P.; Kerszulis, J.; Mahmoud, M.; El-Sayed, M.; Reynolds, J.; Tsukruk, V. *ACS Nano* **2014**, *8*, 6182−6192.
(21) Brown, A.; Sheldon, M.; Atwater, H. *ACS Photonics* **2015**, *2*, 459−464.
(22) Huang, F.; Baumberg, J. *Nano Lett.* **2010**, *10*, 1787−1792.
(23) Hoang, T.; Mikkelsen, M. *Appl. Phys. Lett.* **2016**, *108*, 183107.
(24) Yang, A.; Hoang, T.; Dridi, M.; Deeb, C.; Mikkelsen, M.; Schatz, G.; Odom, T. *Nat. Commun.* **2015**, *6*, 6939.
(25) Ding, T.; Sigle, D.; Zhang, L.; Mertens, J.; de Nijs, B.; Baumberg, J. *ACS Nano* **2015**, *9*, 6110−6118.
(26) Ding, T.; Rüttiger, C.; Zheng, X.; Benz, F.; Ohadi, H.; Vandenbosch, G.; Moshchalkov, V.; Gallei, M.; Baumberg, J. *Adv. Opt. Mater.* **2016**, *4*, 877−882.
(27) Baudrion, A.-L.; Perron, A.; Veltri, A.; Bouhelier, A.; Adam, P.-M.; Bachelot, R. *Nano Lett.* **2013**, *13*, 282−286.

DOI: 10.1021/acs.nanolett.7b04109
Nano Lett. 2018, 18, 853−858

(28) Schwartz, T.; Hutchison, J.; Genet, C.; Ebbesen, T. *Phys. Rev. Lett.* **2011**, *106*, 196405.
(29) Zheng, Y.; Kiraly, B.; Cheunkar, S.; Huang, T.; Weiss, P. *Nano Lett.* **2011**, *11*, 2061.
(30) Pala, R.; Shimizu, K.; Melosh, N.; Brongersma, M. *Nano Lett.* **2008**, *8*, 1506−1510.
(31) Lassiter, B.; McGuire, F.; Mock, J.; Ciracì, C.; Hill, R.; Wiley, B.; Chilkoti, A.; Smith, D. *Nano Lett.* **2013**, *13*, 5866−5872.
(32) Chikkaraddy, R.; Zheng, X.; Benz, F.; Brooks, L.; de Nijs, B.; Carnegie, C.; Kleemann, M.-E.; Mertens, J.; Bowman, R.; Vandenbosch, G.; Moshchalkov, V.; Baumberg, J. *ACS Photonics* **2017**, *4*, 469.
(33) Akselrod, G. M.; Huang, J.; Hoang, T. B.; Bowen, P. T.; Su, L.; Smith, D. R.; Mikkelsen, M. H. *Adv. Mater.* **2015**, *27*, 8028−8034.
(34) Tork, A.; Boudreault, F.; Roberge, M.; Ritcey, A. M.; Lessard, R. A.; Galstian, T. V. *Appl. Opt.* **2001**, *40*, 1180−1186.
(35) Klajn, R. *Chem. Soc. Rev.* **2014**, *43*, 148−184.
(36) Cai, T.; Bose, R.; Solomon, G.; Waks, E. *Appl. Phys. Lett.* **2013**, *102*, 141118.
(37) Sridharan, D.; Waks, E.; Solomon, G.; Fourkas, J. *Appl. Phys. Lett.* **2010**, *96*, 153303.
(38) Herder, M.; Schmidt, B. M.; Grubert, L.; Pätzel, M.; Schwarz, J.; Hecht, S. *J. Am. Chem. Soc.* **2015**, *137*, 2738−2747.
(39) Buback, J.; Kullmann, M.; Langhojer, F.; Nuernberger, P.; Schmidt, R.; Würthner, F.; Brixner, T. *J. Am. Chem. Soc.* **2010**, *132*, 16510−16519.

DOI: 10.1021/acs.nanolett.7b04109
Nano Lett. 2018, 18, 853−858